Giant pressure-induced volume collapse in the pyrite mineral MnS_2

Simon A. J. Kimber[a,1,2], Ashkan Salamat[a,b,1,2], Shaun R. Evans[a,c], Harald O. Jeschke[d,1,2], Kaliappan Muthukumar[d], Milan Tomić[d], Francesc Salvat-Pujol[d], Roser Valentí[d], Maria V. Kaisheva[e], Ivo Zizak[f], and Tapan Chatterji[g]

[a]European Synchrotron Radiation Facility, BP 220, 38043 Grenoble Cedex 9, France; [b]Lyman Laboratory of Physics, Harvard University, Cambridge, MA 02138; [c]Departement für Chemie und Biochemie, Universität Bern, CH-3012 Bern, Switzerland; [d]Institut für Theoretische Physik, Goethe-Universität Frankfurt, 60438 Frankfurt am Main, Germany; [e]School of Chemistry, University of Edinburgh, Edinburgh EH9 3JJ, United Kingdom; [f]Helmholtz-Zentrum Berlin für Materialien und Energie, Berliner Elektronenspeicherring-Gesellschaft für Synchrotronstrahlung-II, Wilhelm Conrad Röntgen Campus, 12489 Berlin, Germany; and [g]Institut Max von Laue-Paul Langevin, BP 156, F-38042 Grenoble Cedex 9, France

Edited by Roald Hoffmann, Cornell University, Ithaca, NY, and approved February 14, 2014 (received for review October 6, 2013)

Dramatic volume collapses under pressure are fundamental to geochemistry and of increasing importance to fields as diverse as hydrogen storage and high-temperature superconductivity. In transition metal materials, collapses are usually driven by so-called spin-state transitions, the interplay between the single-ion crystal field and the size of the magnetic moment. Here we show that the classical $S=\frac{5}{2}$ mineral hauerite (MnS_2) undergoes an unprecedented ($\Delta V \sim 22$ %) collapse driven by a conceptually different magnetic mechanism. Using synchrotron X-ray diffraction we show that cold compression induces the formation of a disordered intermediate. However, using an evolutionary algorithm we predict a new structure with edge-sharing chains. This is confirmed as the thermodynamic ground state using in situ laser heating. We show that magnetism is globally absent in the new phase, as low-spin quantum $S=\frac{1}{2}$ moments are quenched by dimerization. Our results show how the emergence of metal–metal bonding can stabilize giant spin-lattice coupling in Earth's minerals.

Magnetism plays an important role in determining the properties of the minerals that make up Earth's crust and mantle (1, 2). This is due to the ubiquity of transition metals (notably Fe) with unpaired electrons. Under geological pressures, these may undergo abrupt volume collapses due to spin-state transitions. These occur when the crystal field splitting Δ, competes with Hund's rule and electronic Coulomb repulsion to determine the size of the magnetic moment. High pressure can thus make a high-spin (e.g., $S=\frac{5}{2}$) state unstable with respect to a low-spin state (1–5), because Δ increases as the metal–ligand bond distances decrease. For simple materials, volume collapses of $\Delta V \simeq 5\,\%$ are regarded as notable (3–9). Understanding the mechanisms (5) of such magnetically driven transitions, and predicting the high-pressure structures, is ultimately of great importance for modeling the mantle in particular.

The simple pyrite-structured mineral hauerite (10) (MnS_2) was reported nearly 30 years ago to undergo a pressure-induced transition (11, 12). The pyrite structure (13) (Fig. 1*A*) is cubic, with molecular disulfide S_2^{2-} groups, which octahedrally coordinate an fcc lattice of Mn^{2+} sites. Under ambient conditions, a high-spin $t_{2g}^3 e_g^2$ $S=\frac{5}{2}$ moment is stabilized by Hund's rule coupling, and long-range magnetic order results (10). Early work on MnS_2, which used laboratory energy-dispersive diffraction (11), detected a structural change at 11 GPa. These results were interpreted as a spin-state transition to a $t_{2g}^5 e_g^0$ $S=\frac{1}{2}$ state in the marcasite structure. This was supported by later calculations (14). However, when the experiment was repeated using synchrotron radiation (12), an unidentified disordered phase was observed. Together with the large estimated volume collapse (~15%), this little-remarked-upon finding was one of the motivations for the present work.

We used the same natural sample as previous investigations (11, 12), and confirmed its purity by diffraction and X-ray fluorescence measurements (15) (Fig. S1). Pressure was applied using gas-loaded diamond anvil cells. Up to 11.7 GPa, X-ray diffraction (Fig. 1*B*) shows that the cubic $Pa\bar{3}$ pyrite structure is preserved, with no reduction in crystallinity and a low bulk modulus of B = 65.9(3) GPa and B′ = 5.1(2). Upon exceeding 11.85 GPa, a complete switch occurs. The resolution-limited pyrite peaks are replaced by a series of broad maxima, which render structural analysis impossible. The diffraction pattern continues to evolve up to 29.1 GPa, suggesting a substantial region of phase coexistence. Due to the poor quality of the diffraction data on cold compression, we undertook structure searching using density functional theory (DFT) methods. Structure relaxation using Vienna ab initio simulation package (VASP) yielded low-spin metallic pyrite structures as reported previously (14). However, this could not explain the complex diffraction patterns observed. We therefore used (16, 17) the Universal Structure Predictor: Evolutionary algorithm package (USPEX) to generate and compare a large number (*ca.* 2,800) of possible structures. Candidates were locally relaxed using the VASP implementation (18–21) of DFT within the generalized gradient approximation (22). This procedure (23) yielded the (dynamically stable; Fig. S2) arsenopyrite structure shown in Fig. 2*A*. The disulfide dimers are maintained, although the connectivity of the MnS_6 octahedra is dramatically changed with the formation of one-dimensional edge-sharing chains. This structure search was completely ab initio, with no experimental input.

Significance

Minerals that contain magnetic metals may collapse under the pressures found in the Earth's mantle. These so-called spin-state transitions are due to the reduction of the magnetic moment associated with each metal atom. Here we report the discovery of a giant volume collapse in the mineral hauerite (MnS_2) under pressure. Instead of a change in the single-ion magnetic moments, this is driven by the Mn^{2+} cations spontaneously forming pairs, or dimers. In contrast to the magnetic, unpaired electrons found at ambient pressure, the dense new phase contains an ordered arrangement of chemical bonds that are globally nonmagnetic. This "squeezing out" of magnetism is shown to stabilize the huge increase in density.

Author contributions: S.A.J.K., A.S., H.O.J., R.V., and T.C. designed research; S.A.J.K., A.S., S.R.E., H.O.J., K.M., M.T., F.S.-P., R.V., and I.Z. performed research; S.A.J.K., A.S., S.R.E., H.O.J., K.M., M.T., F.S.-P., R.V., and M.V.K. analyzed data; H.O.J. and R.V. contributed new reagents/analytic tools; and S.A.J.K., A.S., H.O.J., and R.V. wrote the paper.

The authors declare no conflict of interest.

This article is a PNAS Direct Submission.

[1]S.A.J.K., A.S., and H.O.J. contributed equally to this work.

[2]To whom correspondence may be addressed. E-mail: kimber@esrf.fr, jeschke@itp.uni-frankfurt.de, or salamat@physics.harvard.edu.

This article contains supporting information online at www.pnas.org/lookup/suppl/doi:10.1073/pnas.1318543111/-/DCSupplemental.

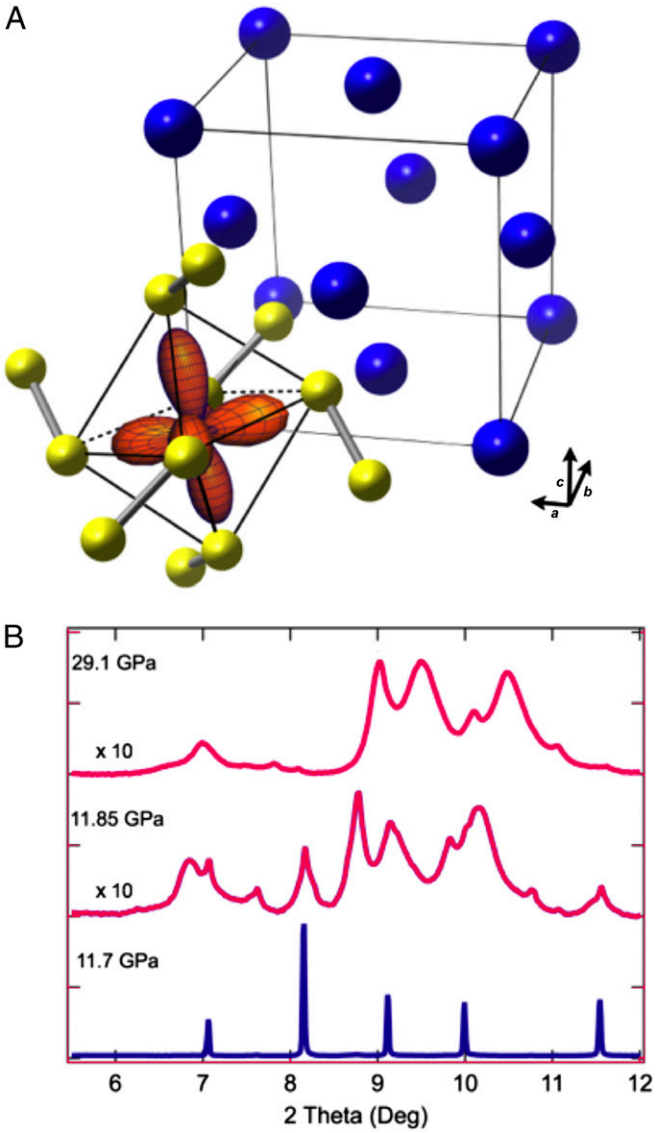

Fig. 1. Ambient pressure structure of MnS_2 and pressure evolution of diffraction profile. (*A*) Perspective view of the structure of pyrite MnS_2, highlighting the fcc lattice of Mn sites (blue spheres) and the disulfide units (yellow dumbbells). The octahedral coordination and the valence e_g orbitals are highlighted for one site. (*B*) Pressure evolution of the X-ray diffraction profile of MnS_2 at ambient temperature showing the collapse into a poorly crystalline phase. Note that the data sets above 11.7 GPa have been multiplied by a factor of 10 for clarity.

To experimentally validate these results, we applied in situ CO_2 laser heating to the disordered state at 20 GPa. In a matter of seconds (Fig. S3), sharp peaks appeared, persisting to our maximum temperature of ~1,800 K. When the laser was switched off, we obtained a phase-pure diffraction pattern. This was indexed with a primitive monoclinic cell, equivalent to that given by our USPEX calculations, in space group $P2_1/c$ with $\beta \sim 111°$, and Rietveld refinement of the arsenopyrite structure proceeded smoothly (Fig. 2*B*). A notable distortion of the edge-sharing chains was found in the refined and calculated structures (Fig. 2*C*). Alternate manganese sites are displaced to form dimer pairs, with a large variation in Mn–Mn distances from 2.72 to 3.42 Å.

The arsenopyrite phase was stable on decompression (Fig. S4) to 6 GPa, before a mixed-phase region, then complete reversion to pyrite was observed. Comparison with the pyrite cell volume at 11 GPa showed a 22% reduction in volume (Fig. 3*A*). This is by far the largest reversible volume collapse reported for any transition metal oxide or sulfide. Upon further decompression into the region of coexistence with pyrite below 6 GPa, the volume difference peaks at around 25%. At ambient conditions, the recovered pyrite lattice parameter was identical to that before compression. We confirmed the stability of the pyrite and arsenopyrite phases independently, by calculating their relative enthalpies. A crossover at 10 GPa is found (Fig. 3*B*), in excellent agreement with experiment.

A change in the spin state of MnS_2 should be reflected in the bond lengths. However, extracting this information from experiment alone is difficult, due to the low-symmetry and texture effects on decompression (Fig. S5). We therefore calculated the pressure dependence of the Mn–Mn and Mn–S distances in both the pyrite and arsenopyrite structures. As shown in Fig. 3 *C* and *D*, a large reduction in the Mn–Mn distances is found at the pyrite→arsenopyrite transition. We also reproduced the dimerization in the edge-sharing chains. This can be seen to be enhanced under pressure, with a marked increase above 16 GPa. When we compared these results with those extracted from Rietveld refinement (24) against the experimental data, we found near-perfect agreement. Similar excellent agreement can be seen for the important ⟨Mn–S⟩ distance. This should be expanded when e_g electron density is present (in the pyrite phase), and contract in a putative $t_{2g}^5 e_g^0$ low-spin state. This exact change in the ⟨Mn–S⟩ distances is found in theory and experiment with a contraction from 2.45→2.24 Å.

We used a range of DFT methods to analyze the electronic structures of both phases of MnS_2 in more detail (25, 26). At ambient pressure, our results for the pyrite structure are similar to those previously reported (14). Type-III antiferromagnetic order (10) is lowest in energy and the calculated band gap is 1.3 eV. A large Mn spin polarization is evident in the electronic density of states (DOS) (Fig. 4*A*), consistent with an $S=\frac{5}{2}$ moment. For the arsenopyrite structure (Fig. 4*B*), a slightly reduced band gap (1 eV) is obtained, however, the highlighted density of states for Mn in the spin-up and spin-down channels is almost identical, showing that the moment has collapsed. The full pressure dependence of the magnetic moment is shown in Fig. 4*C*. This unambiguously shows that the volume collapse in MnS_2 is of magnetic origin. In addition, the correlation between the Mn–Mn dimerization, moment quenching, and band gap (Fig. S6) is demonstrated by the further drop at 16 GPa.

The above results show that the size of the volume collapse in MnS_2 not only exceeds that of previously reported electronic effects, including the benchmark example of cerium (6), but is comparable to the volume drop found when open-framework materials chemically decompose (27). This explains why a kinetically hindered intermediate conceals (12) the thermodynamic ground state on isothermal compression. Unlike other classic examples of pressure-induced spin-state transitions (5), there is no ambiguity about the role of band structure effects, as the arsenopyrite phase of MnS_2 is insulating (Fig. 4*B*). However, the dimerized superstructure that emerges deserves further comment. Isoelectronic $CoSb_2$ also crystallizes with the arsenopyrite structure at ambient pressure, however, on warming above 650 K, the dimer distortion is lost, and a magnetic susceptibility develops (28). Although this has been discussed within the framework of a Peierls-type distortion (29), our calculations show that MnS_2 is actually better described as a 3D network of dimers. The hopping parameters, t, extracted from our electronic structure calculations (Fig. S7) are comparable ($\lesssim 0.15$ eV) in all crystallographic directions, with the notable exception of the intradimer hopping (0.37 eV). The ordered pattern of short Mn–Mn distances thus corresponds to formation of a valence

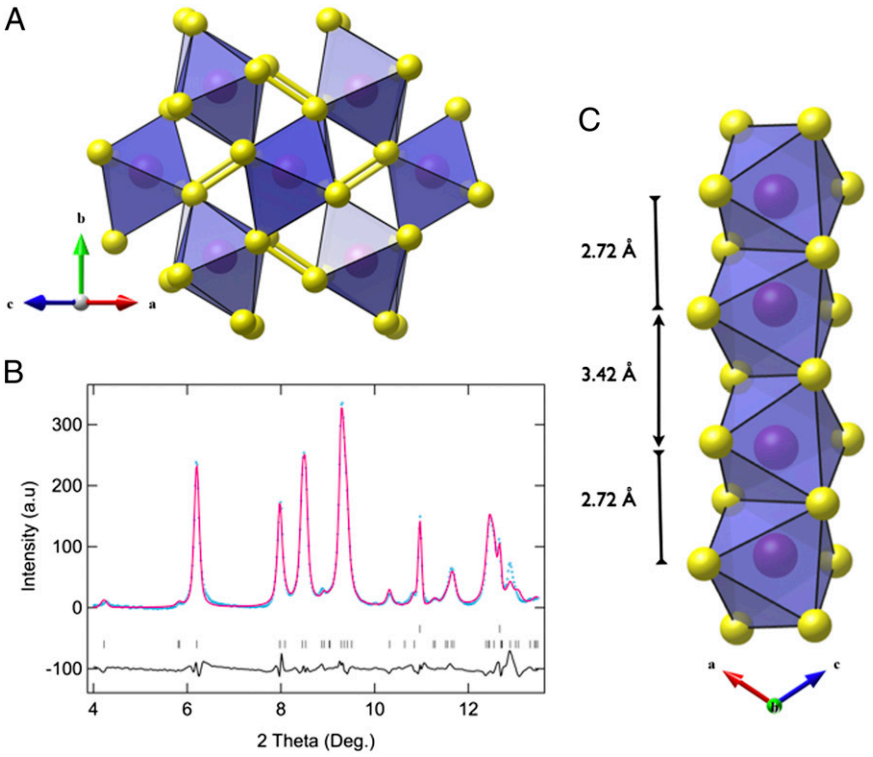

Fig. 2. High-pressure structure and powder diffraction profile of MnS_2. (*A*) Projection of the arsenopyrite high-pressure structure of MnS_2, as predicted by USPEX and as refined against the diffraction profile shown below. This viewpoint is down the chains of edge-sharing MnS_6 octahedra and the arrows indicate the direction of the cell axes. (*B*) Observed, calculated, and difference profiles from the Rietveld fit to the X-ray diffraction pattern of $P2_1/c$ MnS_2 at 20 GPa after laser heating. (*Lower*) Tick marks shows the arsenopyrite peak positions and (*Upper*) peak positions for the neon pressure medium. The refinement converged with $w_{rp} = 0.0985$, $r_p = 0.0706$ and gave cell parameters a = 5.4642(6), b = 5.3742(5), c = 5.4203(7) Å, and $\beta = 111.93(2)°$. See Tables S1 and S2 for more details. (*C*) View of the edge-sharing chains in the refined arsenopyrite structure showing the Mn–Mn dimerization. This viewpoint is perpendicular to that shown in *A*, and the arrows are as before.

bond solid (30). This ground state corresponds to S = 0 Mn–Mn dimers formed by $S = \frac{1}{2}$ Mn ions. Such a ground state is disfavored by larger atomic spins. In $CrSb_2$, which is S = 1, the edge-shared chains remain undistorted, instead showing one-dimensional spin-wave excitations (31). Valence-bond solid formation in MnS_2 is therefore strongly linked to the quantum nature of

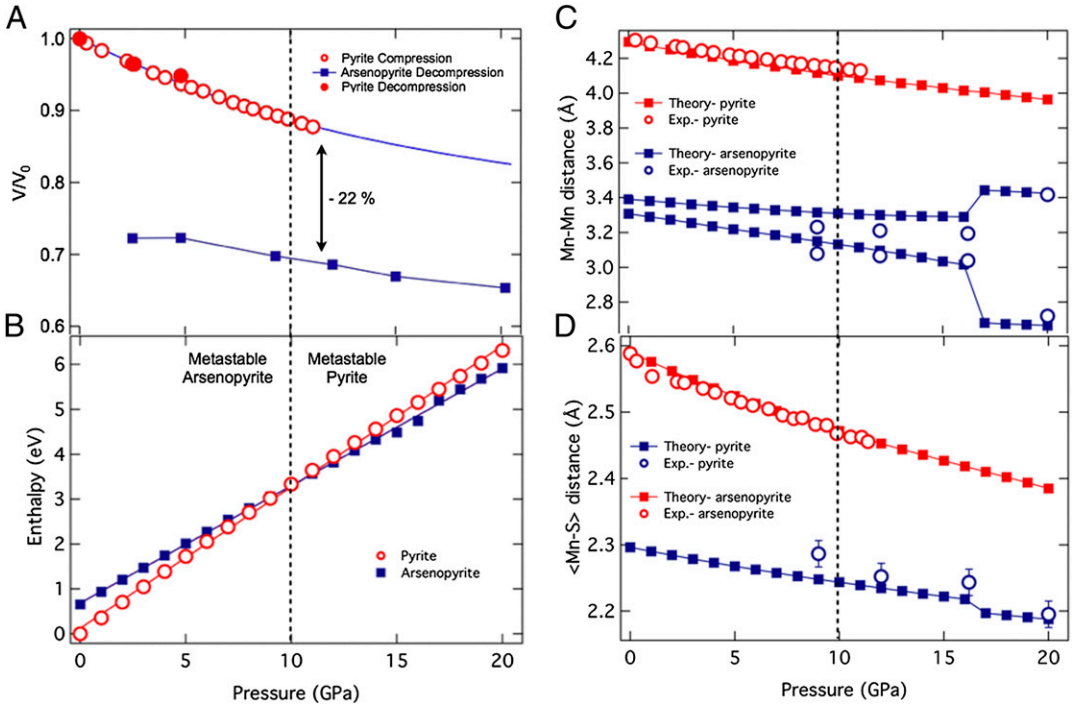

Fig. 3. Pressure evolution of the unit cell volume, enthalpy, and principal bond distances in MnS_2. (*A*) Evolution of the refined unit cell volumes (symbols) of the pyrite and arsenopyrite phases. A fit of a Birch–Murnaghan equation of state to the former is shown as a blue line. (*B*) Pressure dependence of the calculated enthalpy for the pyrite and arsenopyrite phases, showing the metastable regions for both. (*C*) Pressure dependence of the Mn–Mn distances for MnS_2, as extracted from our structure optimizations (filled symbols) and Rietveld refinements (open symbols). (*D*) Pressure dependence of the ⟨Mn–S⟩ distance for both phases of MnS_2. The symbols are as above.

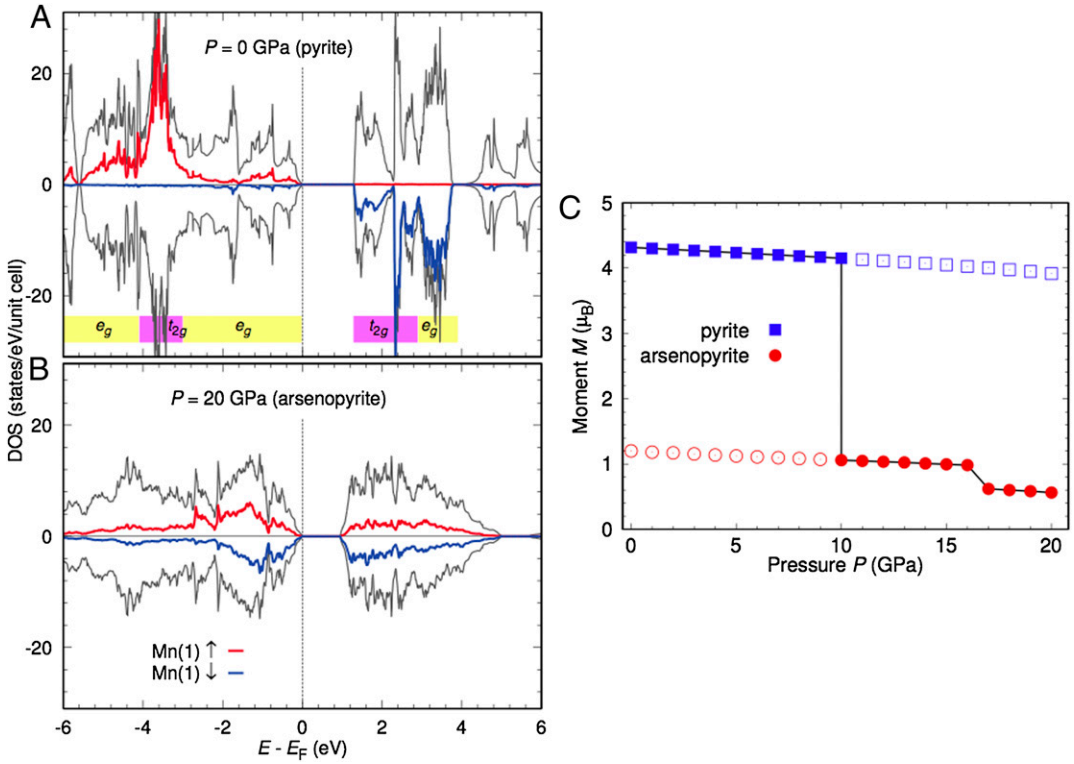

Fig. 4. Pressure dependence of the electronic structure and magnetic moment of MnS_2. (*A*) Spin-polarized electronic density of states for pyrite structured MnS_2 at 0 GPa. The contributions of Mn t_{2g} and e_g states are highlighted and the black line is the total d.o.s. (*B*) Spin-polarized electronic density of states for arsenopyrite structured MnS_2 at 20 GPa. Note the near absence of spin polarization (compare the red and blue lines). (*C*) Pressure evolution of the magnetic moment in MnS_2 as calculated by DFT methods. Clear anomalies can be seen at the volume collapse at 11 and at 16 GPa, where the Mn–Mn dimerization is enhanced.

the $S=\frac{1}{2}$ low-spin state of Mn that is favored by high-pressure conditions.

We believe that the giant volume collapse, as well as the total loss of magnetic moments without metallization, is therefore the result of a quantitatively new mechanism, which goes beyond the simple single-ion paradigm for transition metal materials (32). Although crystal field changes are important, the ultimate stabilizing factor is the surprising formation of dimer interactions in a continuous network solid. The resulting metal–metal bond enthalpy presumably outweighs the cost of the huge increase in density in the arsenopyrite phase. Finally, we note that MnS_2 is geologically scarce; however, the mechanism that stabilizes the volume collapse is valid for more abundant minerals containing isoelectronic cations such as Fe^{3+}.

Methods

A natural single crystal was obtained from the collection of the late Prof. H.-G. von Schnering. This sample is believed to have been acquired from the Mineralogisches Museum Münster *ca.* 1982. A small piece was cracked off and ground into a fine powder for the measurements reported here. The sample was characterized by high-resolution synchrotron powder X-ray diffraction using ID31 (E_i = 31 KeV) at the European Synchrotron Radiation Facility (ESRF), Grenoble, and by X-ray fluorescence measurements at the MySpot beamline of the Berliner Elektronenspeicherring-Gesellschaft für Synchrotronstrahlung (BESSY) II synchrotron, Berlin. All diffraction data were analyzed using the General Structure Analysis System suite of software. The XRF spectra were fitted using PyMca (15).

High-pressure diffraction data were acquired using beam lines ID9A (E_i = 30 KeV) and ID27 (E_i = 33 KeV) at the ESRF. Mar555 and Mar135 CCD detectors were used respectively. The high-pressure experiments were carried out in membrane-driven diamond anvil cells using 300-μm diamonds and rhenium gaskets. For the ambient-temperature compression runs, helium was used as the pressure transmitting medium, and for the laser heating experiments at high-pressure neon was used, which also acted as a thermal insulator. The pressure was calibrated using the recalibrated ruby fluorescence scale (33). Laser heating was carried out in situ at ID27 using a CO_2 laser (λ = 10.6 μm) and the synthesis processed monitored with X-rays. Temperature was calculated from the thermal emission measurements collected from the hotspot of the CO_2 laser irradiation and fitted to either a Planck or Wein function.

We used evolutionary algorithms (USPEX) developed by A. Oganov and coworkers (16, 17) to perform an unbiased search for the high-pressure structure of MnS_2. Each generation contained between 10 and 25 structures, and the first generation was always produced randomly. All structures were locally optimized during structure search using DFT with the projector augmented wave (PAW; ref. 21) as implemented (18–20) in VASP. The generalized gradient approximation (GGA; ref. 22) in the parameterization of Perdew et al. was used as approximation for the exchange and correlation functional.

Based on the P = 0 GPa pyrite and P = 20 GPa arsenopyrite structures of MnS_2, compression and decompression calculations were performed using the PAW basis (21) as implemented in VASP. The structural optimizations were done using a GGA+U functional for the Mn *3d* states with U = 3 eV and J = 1 eV and type-III antiferromagnetic order. We checked for other magnetic orderings but found them to be always higher in energy. Relaxations under constant pressure were performed using the conjugate gradient algorithm. Relaxations were performed in three subsequent passes, and for all relaxations a 300-eV plane-wave cutoff was used in combination with a 6 × 6 × 4 Monkhorst–Pack k mesh.

We analyzed the electronic structure using two full potential all-electron DFT methods. We performed calculations of the total energy, of the magnetic moments and of the density of states for the relaxed pyrite and arsenopyrite structures using the linear augmented-plane-wave basis set as implemented (25) in the code Wien2K and using the full potential local orbital basis (26) (FPLO). We adopted the GGA approximation to the exchange-correlation functional, using GGA+U functionals for the Mn *3d* orbitals with U = 3 eV and J = 1 eV in the fully localized limit, and type-III antiferromagnetic order. The Wien2k calculations were carried out with 200 k points and RK_{max} = 9, resulting in converged energies within a tolerance of 0.05 eV. The FPLO calculations were performed on a 10 × 10 × 10 k mesh with the same GGA+U functional and magnetic order.

ACKNOWLEDGMENTS. We acknowledge M. Hanfland for assistance on ID9A. We thank E. Gregoryanz, J. S. Loveday, W. Crichton, and P. Bouvier for useful discussions. The Beilstein Institut (through Nanobic) and Deutsche Forschungsgemeinschaft provided financial support through Grant SFB/TR49 (to H.O.J., K.M., M.T., F.S.-P., and R.V.). We also gratefully acknowledge the Centre for Scientific Computing in Frankfurt for computing facilities. We thank the ESRF, Grenoble, and BESSY-II, Berlin for access to synchrotron facilities.

1. Cohen RE, Mazin II, Isaak DG (1997) Magnetic collapse in transition metal oxides at high pressure: Implications for the Earth. *Science* 275(5300):654–657.
2. Lin J-F, Tsuchiya T (2008) Spin transition of iron in the Earth's lower mantle. Phys. *Earth Plan Inter* 170:248–259.
3. Ono S, Kikegawa T, Ohishi Y (2004) High-pressure phase transition of hematite, Fe_2O_3 J. *Phys Chem Solids* 65:1527–1530.
4. Lavina B, et al. (2010) Structure of siderite $FeCO_3$ to 50 GPa and hysteresis of its spin-pairing transition. *Phys Rev B* 82:064110.
5. Kunes J, Lukoyanov AV, Anisimov VI, Scalettar RT, Pickett WE (2008) Collapse of magnetic moment drives the Mott transition in MnO. *Nat Mater* 7(3):198–202.
6. Allen JW, Martin RM (1982) Kondo volume collapse and the γ-α transition in Cerium. *Phys Rev Lett* 49:1106–1110.
7. Vajeeston P, Ravindran P, Vidya R, Fjellvag R, Kjekshus A (2003) Huge-pressure-induced volume collapse in $LiAlH_4$ and its implications to hydrogen storage. *Phys Rev B* 68:212101.
8. Kreyssig A, et al. (2008) Pressure-induced volume-collapsed tetragonal phase of $CaFe_2As_2$ as seen via neutron scattering. *Phys Rev B* 78:184517.
9. Xiao W, Tan D, Xiong X, Liu J, Xu J (2010) Large volume collapse observed in the phase transition in cubic $PbCrO_3$ perovskite. *Proc Natl Acad Sci USA* 107(32):14026–14029.
10. Hastings JM, Elliot N, Corliss LM (1959) Antiferromagnetic structures of MnS_2, $MnSe_2$, and $MnTe_2$. *Phys Rev* 115:13–17.
11. Chattopadhyay T, von Schnering HG (1985) High pressure x-ray diffraction study on p-FeS_2, m-FeS_2 and MnS_2 to 340 kbar: A possible high spin-low spin transition in MnS_2. *J Phys Chem Solids* 46:113–116.
12. Chattopadhyay T, von Schnering HG, Grosshans WA (1986) High pressure x-ray diffraction study on the structural phase transition in MnS2. *Physica B* 139-140:305–307.
13. Momma K, Izumi F (2008) VESTA: A three-dimensional visualization system for electronic and structural analysis. *J Appl Cryst* 41:653–658.
14. Persson K, Ceder G, Morgan D (2006) Spin transitions in the $Fe_xMn_{1-x}S_2$ system. *Phys Rev B* 73:115201.
15. Solé VA, Papillon E, Cotte M, Walter Ph, Susini J (2007) A multiplatform code for the analysis of energy-dispersive X-ray fluorescence spectra. *Spec Acta B* 1:305–307.
16. Oganov AR, Glass CW (2006) Crystal structure prediction using ab initio evolutionary techniques: Principles and applications. *J Chem Phys* 124(24):244704.
17. Glass CW, Oganov AR, Hansen N (2006) USPEX—Evolutionary crystal structure prediction. *Comput Phys Commun* 175:713–720.
18. Kresse G, Hafner J (1993) Ab initio molecular dynamics for liquid metals. *Phys Rev B Condens Matter* 47(1):558–561.
19. Kresse G, Furthmüller J (1996) Efficient iterative schemes for ab initio total-energy calculations using a plane-wave basis set. *Phys Rev B Condens Matter* 54(16):11169–11186.
20. Kresse G, Hafner J (1996) Efficiency of ab-initio total energy calculations for metals and semiconductors using a plane-wave basis set. *Comput Mater Sci* 6:15.
21. Blöchl PE (1994) Projector augmented-wave method. *Phys Rev B Condens Matter* 50(24):17953–17979.
22. Perdew JP, Burke K, Ernzerhof M (1996) Generalized gradient approximation made simple. *Phys Rev Lett* 77(18):3865–3868.
23. Muthukumar K, Valentí R, Jeschke HO (2012) Simulation of structural and electronic properties of amorphous tungsten oxycarbides. *New J Phys* 14:113028.
24. Larson AC, Von Dreele RB (2000) *General Structure Analysis System (GSAS).* Los Alamos National Laboratory Report LAUR. 86-748.
25. Blaha P, Schwartz K, Madsen GKH, Kvasnicka D, Luitz J (2001) WIEN2k, an augmented plane wave + local orbitals program for calculating crystal properties (Karlheinz Scwarz, Techn. Universität Wien, Vienna).
26. Koepernick K, Eschrig H (1999) Full-potential nonorthogonal local-orbital minimum-basis band-structure scheme. *Phys Rev B* 59:1743.
27. Arora AK (2000) Pressure-induced amorphization versus decomposition. *Solid State Commun* 115:665–668.
28. Siegrist T, Hulliger F (1986) High-temperature behaviour of $CoAs_2$ and $CoSb_2$. *J Solid State Chem* 63:23–30.
29. Wijeyesekera SD, Hoffmann R (1983) Marcasites and arsenopyrites: Structure, bonding, and electronic properties. *Inorg Chem* 22:3287–3300.
30. Schmidt M, et al. (2004) Spin singlet formation in $MgTi_2O_4$: Evidence of a helical dimerization pattern. *Phys Rev Lett* 92(5):056402.
31. Stone MB, et al. (2012) Quasi-one-dimensional magnons in an intermetallic marcasite. *Phys Rev Lett* 108(16):167202.
32. Tokura Y, Nagaosa N (2000) Orbital physics in transition-metal oxides. *Science* 288(5465): 462–468.
33. Dewaele A, Loubeyre P, Mezouar M (2004) Equations of state of six metals above 94 GPa. *Phys Rev B* 70:094112.